第 29 卷 第 6 期
2008 年 6 月

焊 接 学 报
TRANSACTIONS OF THE CHINA WELDING INSTITUTION

Vol. 29 No.6
June 2008

铝合金薄壁圆筒纵直缝焊接残余应力数值模拟

周广涛[1]， 刘雪松[1]， 杨建国[1]， 闫德俊[1]， 方洪渊[1, 2]

（1. 哈尔滨工业大学 现代焊接生产技术国家重点实验室，哈尔滨 150001；
2. 沈阳航空工业学院 航天技术研究所，沈阳 110034）

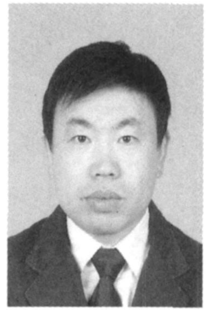

周广涛

摘 要：利用热弹塑性有限元方法对薄壁铝筒纵直焊缝 TIG 焊进行了数值模拟计算，建立了分析模型，定量地描述了准稳态温度场和残余应力场计算数值以及在整个圆筒上的分布情况，并进行了试验验证。结果表明，焊接时热源周围极窄区域温度高、梯度大，离开热源，温度峰值急剧下降；纵向残余应力在焊缝及热影响区为拉应力，最大值位于焊缝长度中心截面上；纵向残余应力在圆周上表现出拉压区交替变化的趋势。利用应力释放法对焊接件进行应力测量，测量结果与模拟计算结果吻合良好。

关键词：数值模拟；温度场；残余应力；应力测量
中图分类号：TG115.28 文献标识码：A 文章编号：0253－360X（2008）06－0089－04

0 序 言

计算机性能的提高和发展，为热弹塑性力学的数值解法开辟了广阔的空间，也使得焊接行为的模拟成了材料加工领域的研究热点。有限元模拟计算可以实现焊接工艺参数从“定性”到“定量”的预测，完成关键物理量的性能评估，节省人力、物力，避免了以往单纯依靠经验、耗费成本的试验来摸索焊接工艺参数的缺点[1－3]。

目前，焊接过程数值模拟计算得到了广泛的应用，目的是揭示焊接本质的规律，因此采用平板对接模拟较多，涉及圆筒焊接模拟的情况比较少[4]，作者利用 MARC 有限元模拟软件，对薄壁圆筒纵向长直缝的焊接过程进行了模拟，定量地描述了圆筒焊接温度场和残余应力场，预测了纵向残余应力在圆筒上各区域的分布规律，为实际焊接生产及变形情况提供参数依据，并从试验上对该结果进行了验证。

1 焊接有限元模型的建立

1.1 网格划分

将模型建成三维实体，模型尺寸为外径 62 mm，壁厚 2 mm，高度 150 mm。为了节省计算时间和提高精度，在温度梯度变化大的焊缝及其附近区域网格加密处理，在离焊缝较远处和温度变化不明显的区域，采用较稀疏的网格，整体上表现为由密到疏的过渡方式。模型如图 1 所示。模型单元为八节点六面体类型，共含 8 880 个单元、13 542 个节点。

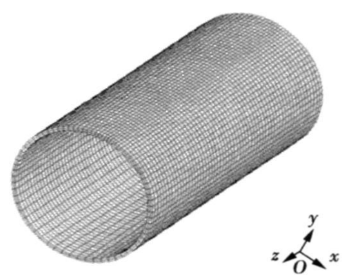

图 1 有限元模型网格划分
Fig 1 FEM mesh model

1.2 热源模型

焊接方法采用 TIG 焊，因此热源采用目前最能接近电弧焊熔池精度的三维双椭球热源模型[5]，如图 2 所示。

前半部分椭球热源表达式为

$$q(x, y, z, t)=\frac{6\sqrt{3}Qf_{\mathrm{f}}}{whc_1\pi\sqrt{\pi}}e^{-3\left[\frac{x^2}{w^2}+\frac{y^2}{h^2}+\frac{(z-v\cdot t)^2}{c_1^2}\right]} \quad (1)$$

后半部分椭球热源表达式为

$$q(x, y, z, t)=\frac{6\sqrt{3}Qf_{\mathrm{r}}}{whc_2\pi\sqrt{\pi}}e^{-3\left[\frac{x^2}{w^2}+\frac{y^2}{h^2}+\frac{(z-v\cdot t)^2}{c_2^2}\right]} \quad (2)$$

收稿日期：2007－10－11

式中:Q 为热源总功率, $Q=\eta IU$, η 为焊接热源热效率; v 为焊接速度; f_f, f_r 为前后椭球热源能量分数, 且 $f_f+f_r=2$; w 为热源半宽; h 为热源深度; c_1 为前半球长度; c_2 为后半球长度。

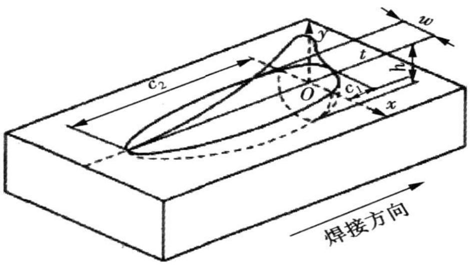

图 2 双椭球热源模型

Fig. 2 Double ellipsoid heat source model

计算时各参数分别为热源效率 $\eta=0.7$, 电流 $I=80$ A, 电压 $U=12$ V, 焊接速度 $v=3$ mm/s, 前半球长度 $c_1=2$ mm, 后半球长度 $c_2=6$ mm, 热源半宽 $w=4$ mm, 热源深度 $h=2.5$ mm, 前椭球热源能量分数 $f_f=1.4$, 后椭球热源能量分数 $f_r=0.6$。

1.3 材料特性

材料的热物理及力学参数是温度的函数, 均随温度而变化, 对于焊接模拟结果准确性有着重要的作用, 模拟采用的材料为 LY12, 性能参数弹性模量 E, 屈服强度 R_{eL}, 热导率 λ, 线膨胀系数 α_l 及比热容 c 随温度变化的情况如图 3 所示。

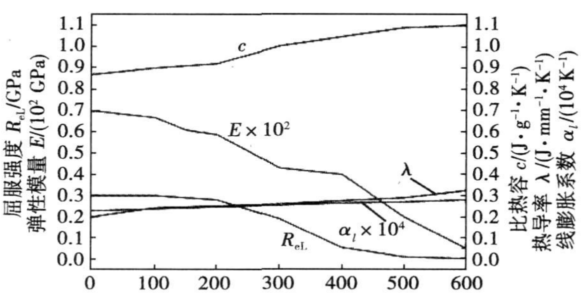

图 3 LY12 材料热—力特征值与温度的关系

Fig. 3 Relationships between thermo-mechanics characteristic and temperature for LY12

2 数值模拟结果

2.1 焊接温度场

温度场是焊接过程首要考虑的参数, 表征了焊件上各点的温度随时间变化过程, 同时也能反映各点瞬时得到的能量。焊件为薄壁件, 单层即可焊透, 模拟时采用单层表面熔敷方式。图 4 给出了当焊接电弧移动到试件中心($x=75$ mm, $t=25$ s)时铝筒瞬态温度场的模拟结果, 如图 5 所示, 可以看出电弧处(熔池)的温度最高, 达到 1 085 ℃, 在电弧前方和后方温度陡降, 温度梯度较大; 在离开焊缝且与之平行的截面上, 温度峰值逐渐降低, 截面上的温度变化也趋于平缓, 在焊缝正对下方的圆筒表面的温度如图 5 中的曲线 5 所示, 各点温度为最低值, 接近室温 20 ℃, 并且保持一致几乎没有变化。可见该铝筒焊接时温度场非常不均匀, 这样的温度分布与圆筒的结构、尺寸特性有关。

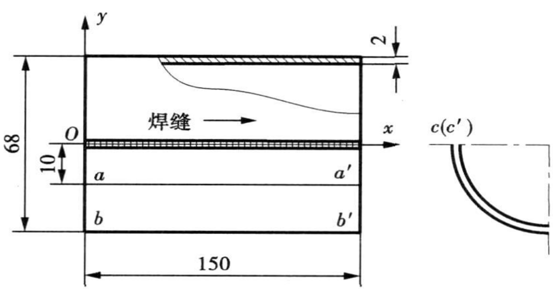

图 4 铝筒尺寸(mm)及分析参照坐标

Fig 4 Analysis coordination for Al cylinder

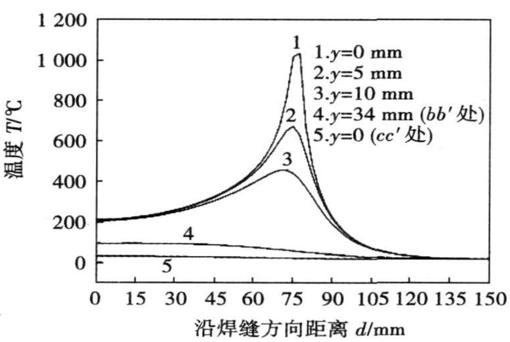

图 5 平行于 x 轴距焊缝不同距离的圆筒面上温度($t=25$ s)

Fig 5 Values of T on cylinder surface along line parallel to x-axis with various lateral distance

模拟结果得出焊缝两侧的温度分布对称, 熔池前方等温线细密, 温度梯度大, 电弧后方等温线比较稀疏, 高温覆盖区域集中, 这将对焊接应力的分布和变形起着决定性的作用。

2.2 焊接应力场

焊接变形和残余应力有着直接的关系, 在此只讨论残余应力场, 图 6 给出了 $x=75$ mm 处圆筒横

截面上纵向残余应力 R_{r1}（平行焊缝长度方向）的分布，可以看出，纵向残余应力以焊缝中心线为中心对称分布。在焊缝所在的上半周筒面上，最大残余应力为 138 MQa，拉应力区很窄，很快过渡到压应力区，最大压应力为－58 MPa，说明塑性区比较窄，这和焊接时温度场的分布有关，电弧移动时，由于铝散热快，电弧周围高温区很窄，在这个区域热应变发展较快，加热膨胀时受到的压缩大，随后冷却受到周围金属的拉伸应力，并残存下来形成残余应力，而下半周筒面上表现出中间为压两边为拉的应力分布规律，但数值很低，参与和上半周应力平衡，如图 6 所示。从焊接瞬态温度场来看，下半圆周上温度低，梯度也不大，因此加热时受到的压缩量不大，因此残余应力较小，$x=R$ 处温度比 $x=0$ 处大，$x=R$ 处为稍许拉应力，大约 8 MPa 左右。

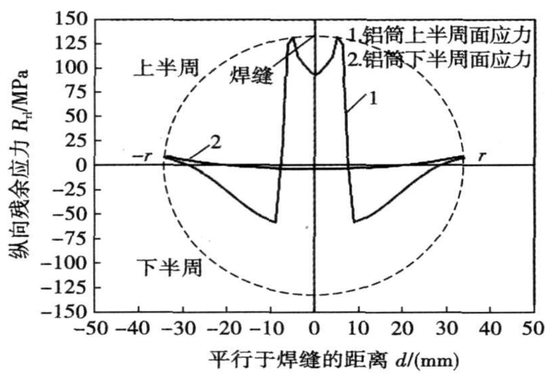

图 6　焊缝中心横截面圆周上纵向应力的布

Fig. 6　R_{r1} at circum of cross-section in middle of weld

平行于焊缝方向过焊缝中心线截面上纵向应力分布如图 7 所示。曲线 1 是经过拉应力峰值点平行焊缝方向纵截面上的纵向残余应力分布，曲线 2 是

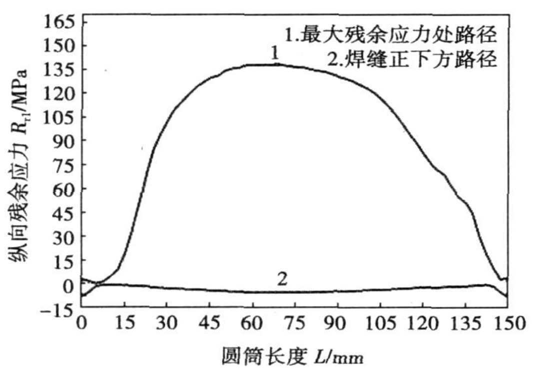

图 7　沿圆筒长度方向纵向应力分布

Fig. 7　R_{r1} distribution along cylinder length direction

焊缝正下方的筒纵截面上的应力。在每个截面上靠近焊缝起点和终点处应力最小，在焊缝中段纵向残余应力有一个稳定的区域，并达到最大值，以过焊缝长度中点截面为中心向两端近似对称分布。其它截面位置上纵向应力幅值介于上述两者之间。随着平行于焊缝方向的距离增加，应力逐渐降低，并表现出和图 8 所示的拉压区交替变化相对应的规律，图中所示的范围分别是各截面位置的最大幅值趋势。

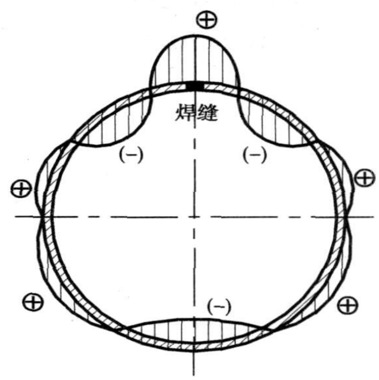

图 8　焊缝横截面纵向残余应力的拉压区示意

Fig. 8　Schematic diagram of tensile-compress region of R_{r1} on weld cross-section

图 8 为该圆筒截面纵向残余应力拉伸—压缩区分布，最大拉应力区在焊缝上，热影响区降为压应力，靠近热影响区的母材金属为较小的拉应力，在离焊缝最远的区域为较小的压应力，最大拉应力距中性轴很近。

3　模拟结果的试验验证

为了验证残余应力计算结果的准确性，进行了实际构件的焊接试验及应力测量。焊接试样与模拟计算采用的尺寸规格一致，材料为 LY12，焊接方法为 TIG 焊，焊接工艺参数为 $I=80$ A，$U=12$ V，$v=3$ mm/s，氩气流量 8 L/min。

应力测量采用应力释放法中的切条法，将需要测量内应力的铝筒划分成几个区域，在各区域的待测点上粘贴应变片，然后在各测点间切出几个梳子状切口，通过静态应变仪测出数值。应变片均匀贴在焊后的铝筒圆周上，如图 9 所示。

测得的纵向残余应力与模拟计算结果的对比如图 10 所示，由于结构的对称性，只测量了一半圆周，可以看出纵向残余应力的模拟计算结果和试验测量

结果基本吻合，除了个别点模拟计算结果比测量结果稍大一点外，证明了模型建立的正确性。

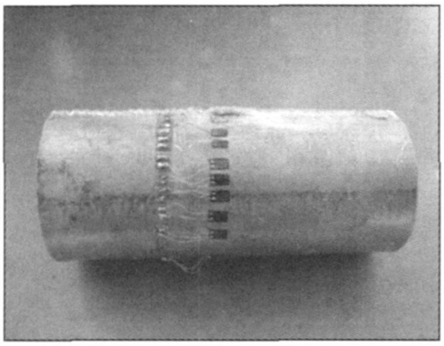

图 9 应变片的粘贴位置

Fig 9 Gluing position of strain gauge

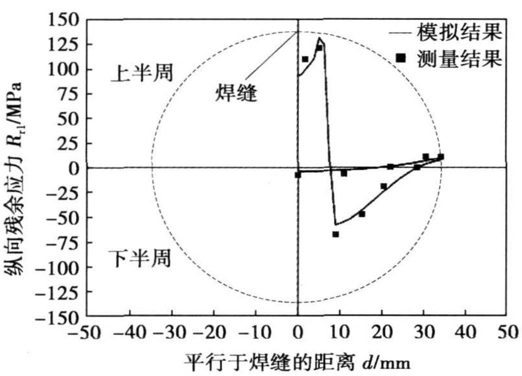

图 10 焊缝中心横截面圆周上纵向残余应力模拟结果和测量结果对比

Fig. 10 Comparison of R_{r1} between simulation and measured results at circum of cross-section in middle of weld

4 结 论

(1) 筒体纵向直缝焊接温度场沿焊缝中心线呈对称分布，焊缝及其附近很窄的区域温度梯度大，远离焊缝温度峰值急剧下降，梯度也趋于平缓，有一大部分还接近室温。电弧前方等温线密集，后方稀疏。

(2) 焊缝中心及周围很窄区域纵向残余应力为拉应力，在焊缝长度中心最大。在整个圆周上拉压应力交替变化，对称分布于焊缝两侧；压应力在圆筒两端及中截面上表现为最大值，之间有个拉压过渡。

(3) 试验测量结果和模拟计算结果进行了比较，两者吻合良好，证明焊接模型建立是正确的。

参考文献：

[1] 宋天虎. 先进制造技术的发展与焊接技术的未来[C] // 第八次全国焊接会议论文集(1). 北京：机械工业出版社，1997.

[2] 汪建华，陆 皓. 焊接预测理论的最新发展[C] // 第八次全国焊接会议论文集(3). 北京：机械工业出版社，1997.

[3] Rosenthal D. Mathematical theory of heat distribution during welding and cutting[J]. Welding Journal, 1941, 20(5): 220s—234s.

[4] Dong Y, Hong J K, Tsai C. Finite element modeling of residual steresses in austenitic stainless steel pipe girth welds[J]. Welding Jonrnal, 1997, 76(10): 442s—449s.

[5] Godak J, Chakravachi A, Malcolm B, *et al*. A new finite model for welding heat source[J]. Metallurgua Transactions, 1984, 15(2): 299—305.

作者简介：周广涛，男，1973 年出生，博士研究生。主要从事焊接结构力学与可靠性分析、裂纹控制和数值模拟研究工作。发表论文 4 篇。

Email：jiaruizhou@yahoo.com.cn

tensile plastic strain in the weld metal is $A\alpha_l(T_m - T_r) - (R_{rt} - R_{rc})/E$.

Key words: welding stress and strain; hypothesis of plain section; compressive plastic strain; tensile plastic strain

Influence of TIG dressing on fatigue property of 10Ni5CrMoV steel welded joints

XUE Gang, WANG Renfu (Luoyang Ship Material Research Institute, Luoyang 471039, Henan, China). p77—80

Abstract: The fatigue tests were taken on the large angle welded joints of 10Ni5CrMoV steel with and without tangsten inert gas welding(TIG) dressing treatment on the toe. The fatigue life, the relation of load and stroke and the fatigue crack initiation at the same loading condition were analyzed comparatively. The welding residual stress was also measured. The stress field and the strain field of welded joints with and without TIG dressing treatment were calculated by the finite element method. The results indicate that the TIG dressing treatment can improve the fatigue property of the large angle welded joints of 10Ni5CrMoV steel. The fatigue life of the welded joints is increased 34% by TIG dressing on the toe at the same loading condition. The primary cause is that the TIG dressing treatment can improve the weld geometry and reduce the stress concentration on the weld toe. So the stress value in the toe is reduced at the same loading condition and the fatigue ability of the welded joints is increased.

Key words: TIG dressing; 10Ni5CrMoV steel; welded joint; fatigue property

Effect of double-wire narrow gap GMA welding parametars on weld appearance

ZHAO Bo, FAN Chenglei, YANG Chunli, ZHANG Liangfeng (1. State Key Laboratory of Advanced Welding Production Technology, Harbin Institute of Technology, Harbin 150001, China). p81—84

Abstracts: The influences of three parameters which are space between wire and edge, space between two wires and angle between two wires on weld appearance were studied in double-wire narrow gap welding with one pool by procedure experiments. The results show that the increase of space between wire and edge can make sidewall penetration and saucer shape of weld surface increase. When the arrangement of wires became parallel, sidewall penetration and saucer shape of weld surface increased to the maximum value. When space between wires increased, sidewall penetration and saucer shape of weld surface increased firstly and then decreased, and finally arrived at peak value when the space between wires is 5—10 mm under the co-action of arc and molten pool energy. But when there was no finger penetration, the three procedure parameters mentioned had little influence on weld penetration. There was lack of fusion of weld bottom when I-shape groove was adopted, and adjusting the three parameters could not eliminate the phenomenon of non-fusion.

Key words: narrow gap welding; twin-wire welding; weld formation

Mechanism and remedy of undercut formation during laser-arc hybrid welding

GAO Ming, ZENG Xiaoyan, HU Qianwu, YAN Jun (Wuhan National Laboratory for Optoelectronics, Huazhong University of Science and Technology, Wuhan 430074, China). p85—88

Abstract: To enhance the reliability of laser-arc hybrid welding, undercut formation and its remedy mechanisms during this process were discussed. The results demonstrated that laser can increase undercut critical speed of hybrid welding, which reaches 5 times than that of arc welding with appropriate welding parameters. Two undercut remedying mechanism resulted from laser-arc interaction were found during hybrid welding. The one is the surface tension state of three phases (solid, liquid and gas) at weld toe is changed by laser-arc synergic effects and form a resultant force pointing to the outside of molten pool. The other is the enhancement of flow speed and time of molten metal flowing from pool center to outer by the increasing of heat input and temperature gradient in molten pool. This faster flow drives molten metal to weld toe and avoid undercut, which is the main mechanism for restraining undercut. Furthermore, the experiential formula to undercut critical speed of hybrid welding and the optimal adjusting range of arc voltage were also obtained.

Key words: laser welding; hybrid welding; undercut; critical speed

Numerical simulation of welding residual stress for longitudinal straight weld seam for aluminum alloy thin-wall cylinder

ZHOU Guangtao[1], LIU Xuesong[1], YANG Jianguo[1], YAN Dejun[1], FANG Hongyuan[1,2] (1. State Key Laboratory of Advanced Welding Production Technology, Harbin Institute of Technology, Harbin 150001, China; 2. Institute of Astronautical Technology, Shenyang Institute of Aeronautical Engineer, Shenyang 110034, China). p89—92

Abstract: Numerical simulation of TIG welding of thin wall aluminum cylinder by thermo-elastic-plasic FEM was conducted. Based on the generation of analysis model, the values and distribution on the whole cylinder for quasi-steady temperature field and residual stress field were described quantitatively. Experiments were performed to verify the residual stress. It can be drawn that during welding there exits high temperature at the centre of heat source and its vicinity where temperature gradient keeps greater. The longitudinal residual stress in weld seam and its HAZ are tensile, its maximum is in the cross-section at the center of weld length and reached 138 MPa. The maximum compressed transverse residual stress was on the both sides of weld seam. The tensile and compressive region of longitudinal residual stress changed alternately at the circumference of cylinder. The residual stress of the welded Al cylinder has been measured by stress-release method, and excellent agreement between the measured value and calculated value is shown.

Key words: numerical simulation; temperature field; residual stress; stress measurement

Laser welding of new type austenite heat-resistant steel HR3C for ultra supercritical boilers

WU Shikai[1], YANG Wuxiong[1], XIAO Rongshi[1], QI Anfang[2], LI Zhongjie[2] (1. Institute of Laser En-